Quantifying uncertainty in flood predictions due to river bathymetry estimation

Martin Nguyen[1, 2, 3], Matthew D. Wilson[1, 3], Emily M. Lane[4], James Brasington[2, 3], and Rose A. Pearson[4]

[1]Geospatial Research Institute, University of Canterbury, Christchurch, New Zealand
[2]Waterways Centre, University of Canterbury, Christchurch, New Zealand
[3]School of Earth and Environment, University of Canterbury
[4]National Institute of Water and Atmospheric Research (NIWA), Christchurch, New Zealand

Correspondence: Martin Nguyen (tmn52@uclive.ac.nz)

Abstract. River bathymetry is important for accurate flood modelling but often unavailable due to the time-intensive and expensive nature of its acquisition. This leads to several proposed and implemented approaches for its estimation. However, the errors in measurements and estimations inherent in these methods, affecting the accuracy of the flood modelling outputs, are not extensively researched. We investigate the sensitivity of flood predictions to these errors in two formulas: the Uniform
5 Flow and the Conceptual Multivariate Regression. Given channel slope, width and bank-full discharge, these formulas can be used to estimate bathymetry. However, errors in estimated bathymetry will affect the flood results. We employed a Monte Carlo framework to introduce random errors into these parameters drawn from a normal distribution with zero mean and a standard deviation set to 10 % of their best estimates. Using this process, we generated 50 simulated river bathymetries for each parameter along with an additional 50 where the errors were applied to all parameters simultaneously. The riverbeds
10 generated from these bathymetries were combined with topographic LiDAR data to create model grids. Each grid was used in the hydrodynamic model LISFLOOD-FP to simulate the 2005 flood event in the Waikanae River area of New Zealand. We assessed the resulting flood predictions for their variability and sensitivity. The results indicate that, between the two methods, the combined errors in the parameters using the Uniform Flow formula are associated with greater uncertainty in flood depths (median error: 3.89 m, quartile range: 2.36 to 7.78 m) and extents (208.72 ha, 206.59 to 209.58 ha), compared to Conceptual
15 Multivariate Regression (depth: 3.61 m, 2.32 to 7.37 m; extent: 207.82 ha, 206.42 to 208.48 ha). Among the parameters, the width errors correspond to the highest uncertainty, while the slope errors correspond to the lowest.

1 Introduction

River bathymetry refers to the river depth measurement (Panigrahi, 2014). It plays a crucial role in flood modelling because it determines when and where water leaves the river channel and starts to flood overland (Cook and Merwade, 2009; Awadallah
20 et al., 2022). Currently, hydrographic surveys and remote sensing methods, especially swath beam sonar and blue-green LiDAR, are prevalently employed to obtain these river bathymetric data (Costa et al., 2009; Kinzel et al., 2013; Dey et al., 2019). Multi-beam sonar is effective but time-consuming, while blue-green LiDAR is faster but unable to obtain

measurements in sediment-laden or deep water (Bailly et al., 2010; Flener et al., 2012; Bures et al., 2019). For these reasons, various approaches have been proposed to estimate these data (Ghorbanidehno et al., 2021; Araújo and Hedley, 2023).

25   Dey et al. (2019) categorized these methods into two groups. The first one assumes rivers with simple geometric shapes like triangular (Gichamo et al., 2012; Saleh et al., 2013; Bhuyian et al., 2015), rectangular (Trigg et al., 2009; Saleh et al., 2013; Grimaldi et al., 2018), trapezoidal (Saleh et al., 2013), or parabolic (Bhuyian et al., 2015) cross-sections. Despite the fast and simple process, these assumptions might be significantly different from realistic rivers. The other group applies more complex hydraulic (Price, 2009; Bhuyian et al., 2015) and geomorphological (Brown et al., 2014) principles to create more realistic

30   underwater terrain. However, they require more data and heavy computation.

    Some studies build up formulas to estimate river bathymetry based on river types. For instance, López et al. (2007) constructed an equation to estimate the discharge for coarse-grained rivers. Rupp and Smart (2007) then developed this into an equation for estimating river depth. More recently, machine learning methods have been used to estimate river bathymetry. For instance, Bures et al. (2019) employed a DEM, flow discharge, Manning's n, and support from Random Forrest to model

35   riverbed topography, while a Deep Neural Network was used by Ghorbanidehno et al. (2021) to map riverbed features from depth-averaged flow speed data.

    Neal et al. (2021) categorized four approaches to solve the lack of bathymetric data in flood modelling cases. The first method involves subtracting the estimated river bank-full discharge from the total floodwater to simulate the 'excess discharge' on the floodplains without requiring bathymetric data (Neal et al., 2012). However, it is expected to become inaccurate over large and

40   complex floodplains (Neal et al., 2012; Sampson et al., 2015). The second method applied the downstream hydraulic geometry (Leopold and Jr, 1953) to estimate riverbed elevation. The relationship between river width, depth, and bank-full discharge used in the method is developed empirically from field observations across many sites (Andreadis et al., 2013; Yamazaki et al., 2013; Gleason and Smith, 2014; Grimaldi et al., 2018). This technique can introduce uncertainties due to various complexities of different rivers into the estimated river (Neal et al., 2021).

45   The third method applies the Manning's n equation with an assumption of uniform channel over long distances. The formula considers river slope, width, discharge, and friction, to estimate the river depth (Coe et al., 2008-07; Miguez-Macho and Fan, 2012; Brêda et al., 2019). However, real-world rivers are often different from uniform flow conditions, which might cause the flood predictions to be larger or smaller than expected. (Neal et al., 2021). In the final method, an observed water surface profile is used to estimate the river bathymetry by applying gradually varied flow equations (Garambois and Monnier, 2015;

50   Brêda et al., 2019; Andreadis et al., 2020). Despite high accuracy, it is resource-intensive and obtaining the necessary data can be challenging and expensive.

    Regardless of the approach, errors in the measurements or estimations can introduce uncertainties that significantly deviate the simulated river bathymetries from the actual ones. Consequently, using these modelled river bathymetries can affect the flood predictions. Currently, only limited studies concentrate on these errors in bathymetry estimation (Durand et al., 2008;

55   Lee et al., 2018; Moramarco et al., 2019; Kechnit et al., 2024).

    Some of the studies have used a Monte-Carlo framework or equivalent methods to generate a range of river bathymetries. For instance, Durand et al. (2008) estimated river bathymetry used for flood modelling by combining synthetic water surface

elevation data from the then-proposed SWOT satellite mission. Within a Monte Carlo framework, they conducted a sensitivity analysis to assess how various error sources affected the estimated results, and found that errors in the river roughness and flow

60 conditions have greater influence than measurement errors in that SWOT data. Nevertheless, their approach did not consider the spatial variability of each parameter.

Moramarco et al. (2019) introduced a method based on the entropy theory (Shannon, 1948) using channel slope, width, bottom elevation, and a parameter from Alessandrini et al. (2013) to model the river depths. These parameters were estimated using an algorithm that can minimize the observed maximum surface velocity (Moramarco and Singh, 2010). Similar to the

65 Monte Carlo approach, for assessing uncertainties from these parameter estimations, the authors created 1000 river depths from 1000 combinations of parameter values randomly selected from uniform distributions. Kechnit et al. (2024) later extended these techniques to estimate river bathymetry and quantifying uncertainties in larger-scale rivers. However, neither study explored the spatial variability of each parameter nor investigated how uncertainty in each parameter estimation influences the river depth as well as flood predictions.

70 Lee et al. (2018) introduced a principal component geostatistical method to produce fast bathymetry maps along with the uncertainties. Nevertheless, without using Monte Carlo framework, their research considered uncertainties arising from velocity measurement errors by adding only four Gaussian errors (0.025, 0.01, 0.05, and 0.1 m/s) to the true values without full assessment of the implications of these errors. Hence, their results might not be fully representative of uncertainties in flood prediction caused by errors in river bathymetry.

75 Generally, these previous studies have addressed certain gaps in quantifying uncertainties in estimated river bathymetry and show that errors can arise from various sources. However, they have not considered the spatial variability of estimated parameters used for river bathymetry generation, or performed a thorough sensitivity analysis to examine the impact of each parameter on the estimated river bathymetry, particularly in flood modelling contexts.

In this paper, we quantified the uncertainty in flood predictions due to errors in estimated parameters used in two formulas

80 described in Rupp and Smart (2007) and Neal et al. (2021). Using a Monte Carlo framework, we generated multiple realizations of river bathymetry, then used this to perform a sensitivity analysis to evaluate the impacts of each parameter on flood predictions, individually and collectively. In the next section, we describe a method to explore relationships between parameters within these two formulas and show a process to examine how errors in these parameters affect the flood predictions.

2   Methodology

In this section, we first introduce the study site, the Waikanae River, and the necessary data. Next, we define two formulas used for river bathymetry estimation and show a method to explore the relationships between parameters and river bathymetry in these two equations. We then show how to examine these relationships based on the river of the study site. Finally, from a workflow, we describe how to introduce errors into the river bathymetry estimations, how they propagate through the flood

90 modelling to the predictions, and how the sensitivity analysis is performed.

2.1 Study site and data source

Similar to Nguyen et al. (2024b), we simulated a fluvial flood event on the Waikanae River, Kaipiti Coast, New Zealand between 5th and 7th January, 2005. Figure 1a depicts our site study extending about 7 km from the Waikanae Water Treatment Plant gauge to the coast. Figures 1b and 1c show the flow information recorded at the gauge by the Greater Wellington Regional Council (2005) and the tidal data estimated by the NIWA Tide Forecaster (2005) respectively.

Following the approach of Nguyen et al. (2024b), the DEM and roughness length in our paper were generated by an open-source Python package, GeoFabrics (version 0.9.4), developed by Pearson et al. (2023). Accordingly, the package sampled and interpolated ground LiDAR data downloaded from OpenTopography (2013) onto a 10-metre square grid using Inverse Distance Weighted – an interpolation method has been commonly used in flood modelling (Ibrahim and Fritsch, 2022; Xing et al., 2022; Huang et al., 2023). Because the LiDAR only contains the water surface elevations, the estimated river bathymetric data were obtained by subtracting the estimated river depths (see Section 2.2) from these water surface elevations. The roughness length was converted to Manning's n using a conversion developed by Smart (2018):

$$n = \frac{kH^{1/6}(\frac{H}{z_o} - 1)}{\sqrt{g}(1 + \frac{H}{z_o}(ln\frac{H}{z_o} - 1))} \tag{1}$$

where z_o is roughness length, n is Manning's n coefficient, k is von Karman's constant (0.41), and H is the flow depth assumed as 1 m in this paper. These DEM and Manning's n were then applied to the LISFLOOD-FP flood model (Bates et al., 2010; Neal et al., 2018), which was calibrated for this site in Nguyen et al. (2024b), to run the flood simulations.

2.2 Method to investigate formulas for river bathymetry estimation

The depths were estimated at regular 10-metre intervals along the river with each point representing an average cross-sectional depth (h). From now on, we will use the river bathymetry as an interchangeable term for the river depth. Two formulas were used for this estimation - the Uniform Flow (UF) (Neal et al., 2021) and the Conceptual Multivariate Regression (CMR) (Rupp and Smart, 2007). The CMR formula was selected to match with the coarse-grained Waikanae River (Gyopari et al., 2014), and the UF formula was chosen for its simplicity (Neal et al., 2021) and can be widely applicable. Both are designed in the GeoFabrics and can be presented through a general equation as below:

$$h = (\frac{nQ}{wS^\beta})^{\frac{1}{1+\alpha}}. \tag{2}$$

The cross-section width (w) at bank-full river and river slope (S) were estimated from LiDAR data as detailed in Pearson et al. (2023). The river bank-full flow (Q) and river Manning's (n) were obtained from Henderson and Collins (2018) at NIWA. For the α and β coefficients, the UF formula used two constant values of 2/3 and 1/2, while the CMR formula applied 0.745 and 0.305 respectively with another constant value of 0.162 for Manning's n. The exponent and value range of each parameter are shown in Table 1. In our research, we assumed the errors in the estimated river bathymetries arising from the errors in these
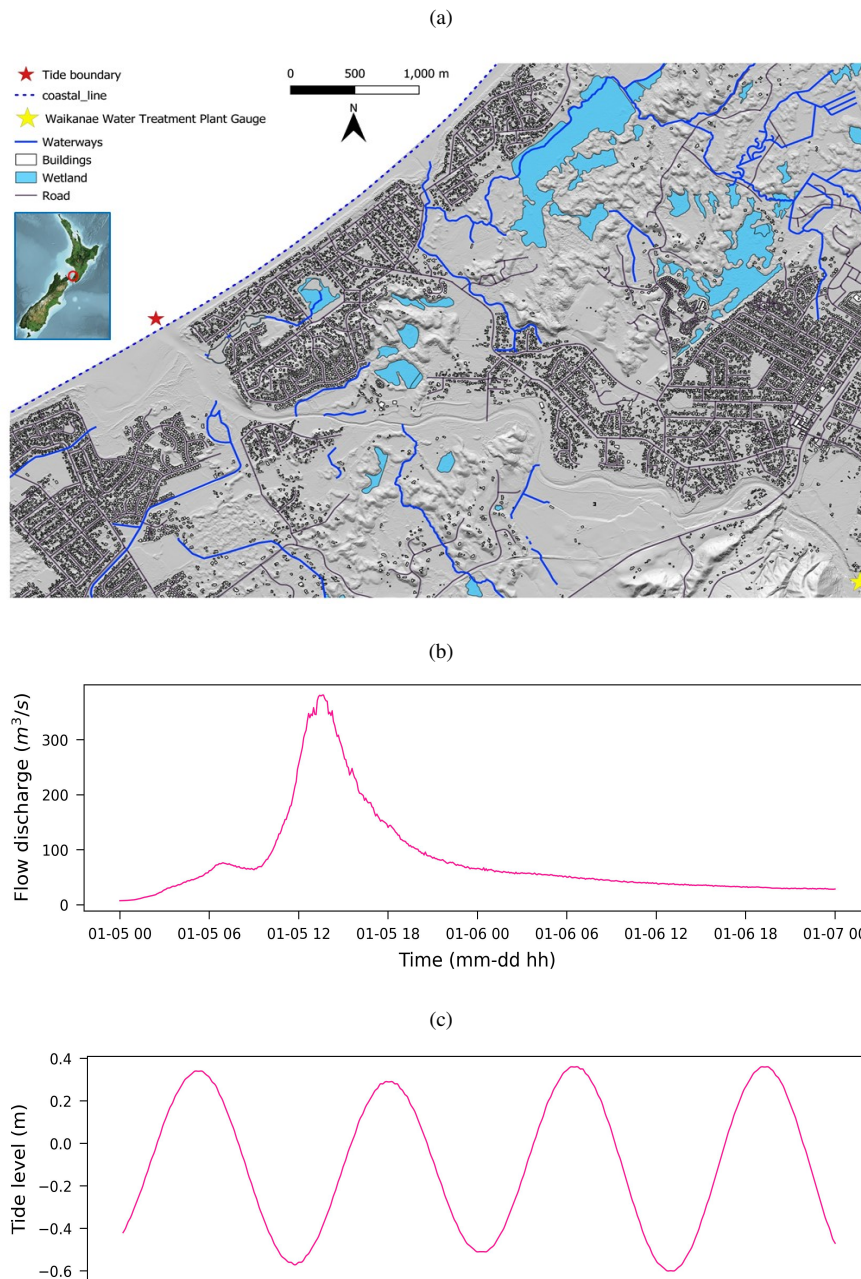
Figure 1. Study site and data source (adapted from Nguyen et al., 2024b): (a) Waikanae River in Kaipiti, New Zealand; (b) the river flow recorded by the (Greater Wellington Regional Council, 2005); and (c) tidal data recorded by the (NIWA Tide Forecaster, 2005) for the flood event from 5th to 7th January, 2005.

Parameters	Slope (S)	Flow (Q)	Width (w)	Manning's n (n)
Exponents – CMR	0.175	0.573	0.573	0.573
Exponents – UF	0.3	0.6	0.6	0.6
Minimum values along the river	0.3 (m/km)	145.3 (cumec)	19.4 (m)	0.162 (for CMR) 0.0377 (for UF)
Maximum values along the river	7.2 (m/km)	146.2 (cumec)	99.6 (m)	0.162 (for CMR) 0.0436 (for UF)
Mean values along the river	4.0 (m/km)	146.1 (cumec)	35.6 (m)	0.162 (for CMR) 0.0433 (for UF)

Table 1. The exponents of parameters in the Conceptual Multivariate Regression and Uniform Flow formulas, and the value ranges (minimum, maximum, and mean) of parameters along the Waikanae River – the river slope, bank-full flow, width, and Manning's n – used to explore their relationships with the river bathymetry in both formulas.

parameters owing to estimation. Due to time-consuming and complex nature of processing simulations for river Manning's n and coefficients α and β, we focused solely on the errors in the river slope, bank-full flow, and width in this paper.

Before Monte Carlo simulation process, we explored the relationship between these parameters and the river bathymetries estimated by the UF and CMR formulas. For each parameter, we took the mean value over the entire river section as seen in Table 1 and investigated how the river bathymetry would change between half (50 %) and twice (200 %) value of each parameter, except for Manning's n. With this same amount of variation between parameters, this method reveals us the relationship between each of them and the river bathymetry.

2.3 Method to evaluate relationships of bathymetry and parameters in the formulas on the study site

We then make the findings of Section 2.2 more concrete by investigating how they play out along the Waikanae River. We look at the best estimates of the parameters (slope, bank-full flow, and width) and the Waikanae River bathymetry along with the Monte Carlo simulations of their variances. Here, we examine how each parameter and their combination along with errors are correlated with the river bathymetry. Specifically, we visualize the variation of each parameter along the river and the resulting variation in river bathymetry. We plot both the values as a function of location along the river and scatter plots of their relationships. We also plot the along-river bathymetries for the combined errors of all three parameters. Three scatter plots depict the relationships between the variance of each parameter and these combined river bathymetries. In the next section, we detail how to generate these simulated parameters and corresponding river bathymetries and examine their variations on flood predictions.
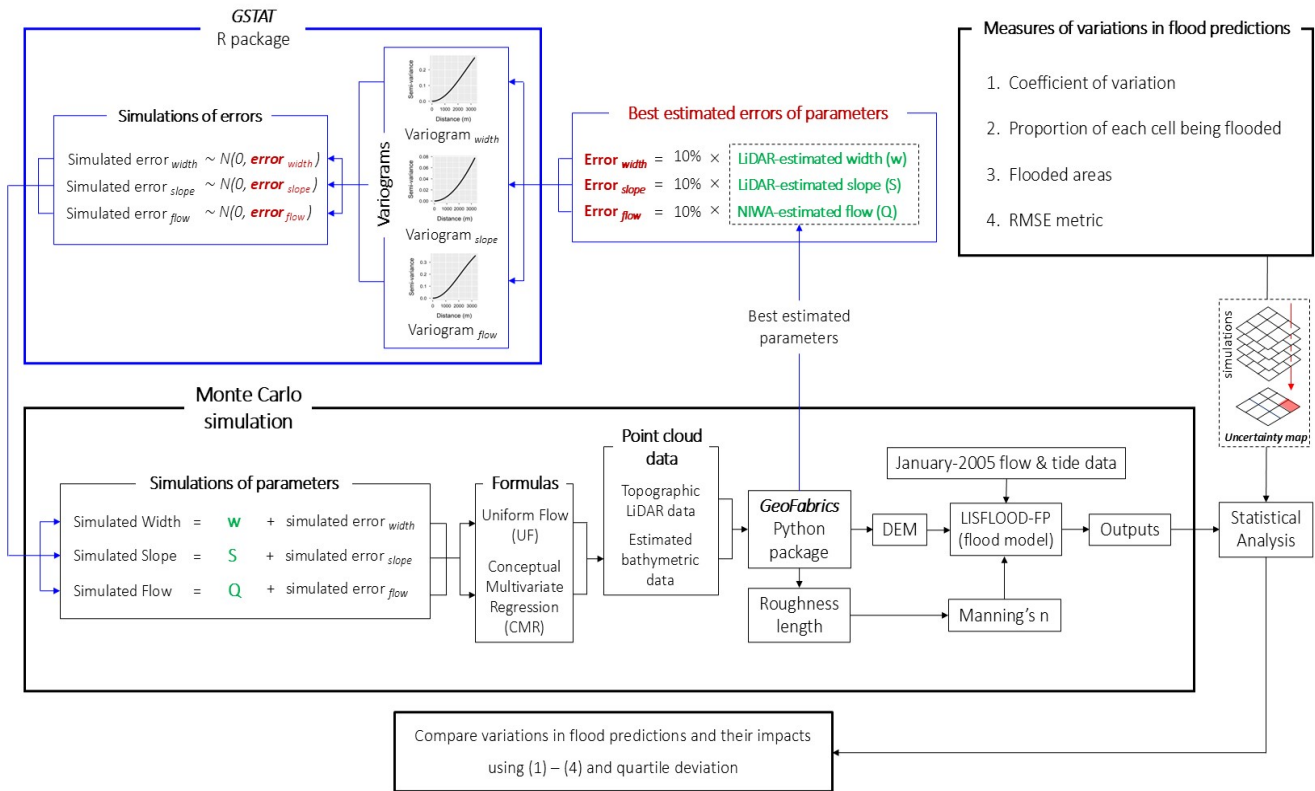
Figure 2. Process to quantify uncertainty in flood predictions using river bathymetries estimated by the Conceptual Multivariate Regression and Uniform Flow formulas, with associated error distributions in parameters: river slope, bank-full flow, and width.

2.4 Monte Carlo simulation process

Figure 2 shows a Monte Carlo simulation process undertaken in this study. At first, to generate multiple simulated parameters with the same amount of errors, we used GeoFabrics package to gather their best estimates along the river derived from LiDAR

140 (river slope and width) and estimated by NIWA (river bank-full flow). We assumed that their expected errors would be 10 % of these best-estimated values. For each parameter, we spatially model the variation of the errors along the river with a Gaussian variogram. This was implemented using Gstat, an open-sourced R package developed by Pebesma (2004); Gräler et al. (2016). The Gaussian variogram was chosen because it smoothly represents how errors might vary over space, ensuring that points closer to each other along the river have more similar errors. This is particularly suitable for river slope, bank-full flow, and

145 width, which tend to change gradually rather than abruptly along the river.

Next, this variogram was employed to generate 50 unconditional simulations of these errors from a normal distribution with a zero mean and a standard deviation equal to the expected error. Each simulation is different along the river but with the same characteristics of the variogram. 50 realizations of each parameter were then generated by adding these simulated errors to the

No.	Dataset names (Parameter – formula)	Descriptions
1	Slope - UF	50 simulated river depths/riverbed elevations estimated by the Uniform Flow formula when the simulated errors selected from N(0, **error$_{slope}$**) were added into the LiDAR-estimated slope
2	Flow - UF	50 simulated river depths/riverbed elevations estimated by the Uniform Flow formula when the simulated errors selected from N(0, **error$_{flow}$**) were added into the NIWA-estimated flow
3	Width - UF	50 simulated river depths/riverbed elevations estimated by the Uniform Flow formula when the simulated errors selected from N(0, **error$_{width}$**) were added into the LiDAR-estimated width
4	Combination - UF	50 simulated river depths/riverbed elevations estimated by the Uniform Flow formula when the simulated errors selected from N(0, **error$_{slope}$**), N(0, **error$_{flow}$**), and N(0, **error$_{width}$**) were simultaneously added into the LiDAR-estimated slope, NIWA-estimated flow, and LiDAR-estimated width respectively
5	Slope - CMR	50 simulated river depths/riverbed elevations estimated by the Conceptual Multivariate Regression formula when the simulated errors selected from N(0, **error$_{slope}$**) were added into the LiDAR-estimated slope
6	Flow - CMR	50 simulated river depths/riverbed elevations estimated by the Conceptual Multivariate Regression formula when the simulated errors selected from N(0, **error$_{flow}$**) were added into the NIWA-estimated flow
7	Width - CMR	50 simulated river depths/riverbed elevations estimated by the Conceptual Multivariate Regression formula when the simulated errors selected from N(0, **error$_{width}$**) were added into the LiDAR-estimated width
8	Combination - CMR	50 simulated river depths/riverbed elevations estimated by the Conceptual Multivariate Regression formula when the simulated errors selected from N(0, **error$_{slope}$**), N(0, **error$_{flow}$**), and N(0, **error$_{width}$**) were simultaneously added into the LiDAR-estimated slope, NIWA-estimated flow, and LiDAR-estimated width respectively

Table 2. Dataset descriptions of simulated river bathymetries estimated by the Uniform Flow and Conceptual Multivariate Regression formulas with errors in parameters: river slope, bank-full flow, and width.

corresponding best estimated parameter. This quantity was chosen for time efficiency as testing with a larger number we found that using more representations did not considerably impact the results.

Here, we selected the normal distribution because we assumed our parameters from the estimations and measurements provide the most accurate values, making them the most probable. Moving further from them, the probability of errors should decrease. Additionally, we presumed the errors can be both negative and positive, balanced around zero. Besides, the lack of information about the true errors led us to use unconditional simulation. This method provides a wide range of errors to understand better their relationships with the river bathymetries and how they impact flood predictions.

Subsequently, 400 realizations (eight datasets of 50 simulations) of the river bathymetries were created in total: 50 representing the variation in each of the three parameters (river slope, bank-full flow, and width) and additional 50 using the combined variations in the three parameters times the two formulas (UF and CMR) used for calculation. Next, these simulated river bathymetries were then subtracted from the LiDAR-estimated water surface elevations to obtain the simulations of riverbed elevations. Eight datasets of these simulated bathymetric data were organized and presented in the Table 2.

Similar to Durand et al. (2008); Moramarco et al. (2019); Kechnit et al. (2024), and especially Nguyen et al. (2024b), our research also applied a Monte Carlo framework to generate 50 DEMs and 50 Manning's n maps with 50 different river bathymetries using the method mentioned in Section 2.1 for each dataset. These data were then used for modelling the January-2005 flood event to produce 50 maximum water depths (MWDs) for further statistical analysis.

165   To assess the uncertainty in flood predictions, we measured the variability in these simulated MWDs by computing their mean (mMWDs) and standard deviation (sdMWDs) to calculate the coefficient of variation (covMWDs). The proportion of simulations in which a given pixel was flooded (pFs) were also computed to distinguish where was always flooded, never flooded, and sometimes flooded throughout these realizations. However, different to (Nguyen et al., 2024b), mMWDs and sdMWDs were not considered in the research due to no useful information.

170   The covMWDs and pFs were then mapped with probability density functions for each set. Here, pixels with mMWDs of 0.1 m or greater were classified as flooded and included in the analysis, while those of shallower than 0.1 m were excluded. Apart from that, the oceanic zone and river were also removed to focus on the variations in the floodplains. Additionally, we computed flooded area, a metric often employed by decision-makers, for each simulation for comparison.

To examine variations in flood predictions of the eight datasets, side-by-side boxplots were applied to visualize the 175   distributions of flood extents and those of covMWDs. We compared the magnitude of their variations using the quartile deviation metric which was also employed by Nguyen et al. (2024b). In our research, we went further than Nguyen et al. (2024b) by validating each flood simulation with the observed flood levels measured by Wallace (2010) for the January-2005 event. The Root Mean Square Error (RMSE) metric was harnessed for these validations. Locations of the observed data where the flood model predicted to be dry across all the simulations were removed to ensure the RMSE focuses only on predicted 180   flooded regions and to avoid skewing the RMSE. We also visualized the distribution of RMSEs across simulations through side-by-side boxplot for comparison.

3 Results

In this section, we showcase the findings from investigating the relationships between the bathymetry and parameters in two formulas, followed by the results from evaluating how these findings playing out with the study site, the Waikanae River. We 185   then illustrate the results from comparing variations in flood predictions across eight datasets.

3.1 Findings from investigating formulas for river bathymetry estimation

Figure 3 shows the relationships between the river bathymetry and three parameters – river slope, bank-full flow, and width. As seen in Fig. 3a, a steeper river is prone to be shallower. This inverse relationship is mathematically represented in both formulas, where the slope appears in the denominator. Physically, it is expected that in steeper sections, where the river width 190   and flow volume do not vary, the water tends to flow faster and spend less time interacting with the riverbed, thereby its force has a smaller impact on the river bathymetry.
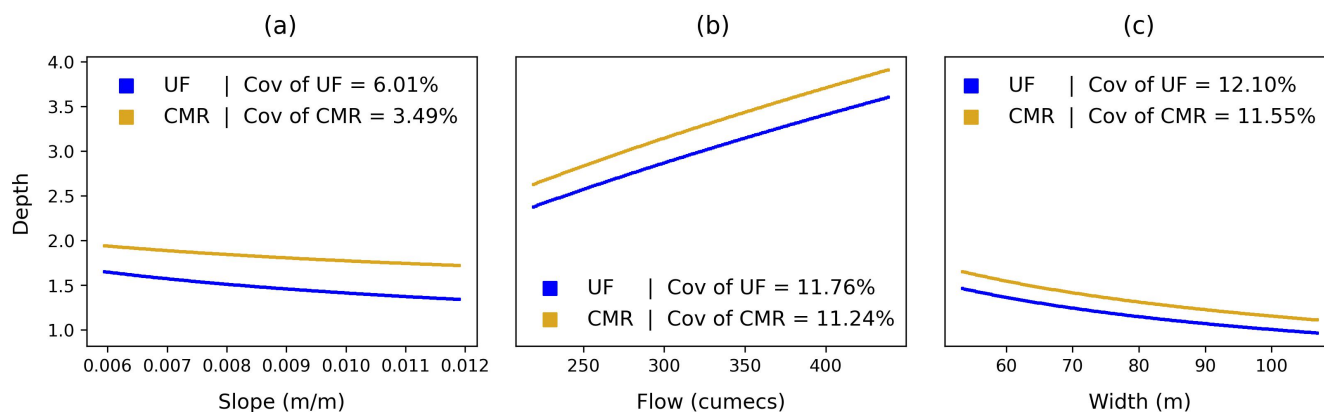
Figure 3. Formula investigation: relationships between (a) river slope, (b) bank-full flow, and (c) width with river bathymetries estimated by the Uniform Flow and Conceptual Multivariate Regression formulas. Each plot shows how the river bathymetries are correlated with increasing the mean value of a parameter (see Table 1) from 50 % to 200 % while keeping others constant.

Figure 3b shows that a deeper river tends to have larger flow. This proportional relationship can be explained mathematically in both formulas, where the flow is in the numerator. Physically, it can be understood that, in the river sections where the river width and slope do not vary, the increased flow has greater water force, which is correlated with a higher impact on the river bathymetry than smaller flow.

Figure 3c depicts that wider river is likely to be shallower. It can be comprehended that in wider river sections, where the river slope is unchanged, the constant water volume spreads out and reduces its force which has a smaller impact on the river bathymetry. This inverse relationship is also presented in both formulas, where the width is positioned in the denominator.

Based on the coefficients of variation, the variations in the river bathymetries are more strongly correlated with the variations in the width than the flow, and much more than the slope. Physically, the width can control the water distribution on the riverbed, which is strongly connected to the impact magnitude of the water force on the river bathymetry. Meanwhile, although higher flow increases the water force, it does not control water distribution as effectively as the width does, which has less correlation with the river bathymetry. The slope is primarily associated with the flow velocity rather than the water distribution, so its changes are much less correlated with the changes in the river bathymetry.

Mathematically, the width and flow have the same higher exponents in both formulas (0.6 for UF, 0.573 for CMR) compared to the slope (0.3 for UF, 0.175 for CMR). This highlights why variations in the width and flow have stronger correlations with the river bathymetry. Additionally, with width in the denominator and flow in the numerator, flow variability is slightly less correlated with the variability in the river bathymetry than width variability.

Apart from that, in Fig. 3, the river bathymetry estimated by the CMR formula is generally greater than that estimated by the UF formula. This difference arises from many factors, but mainly from the friction and its exponent in this case. The mean friction along the river used for the UF formula (0.0432) is lower than the constant friction (0.162) in the CMR formula. Also,

its exponent in the UF formula (0.6) is higher than in the CMR formula (0.573). However, when considering other factors, for instance, if the width continues to increase and the slope or flow decreases, the river bathymetries estimated by both formulas can converge, switch positions, and then diverge again. Besides, based on the CoVs, for the same amount of variation in the parameters, the river bathymetries estimated by the UF formula have higher variability than that estimated by the CMR formula. To explain, the exponents of the slope (0.3), flow (0.6), and width (0.6) in the UF formula are higher than in the CMR formula (0.175, 0.573, 0.573, respectively).

Overall, a steeper or wider river typically becomes shallower, while an increase in the flow corresponds to a deeper river. Moreover, variation in the river width corresponds to the largest variability in the river bathymetry followed by variations in the river flow and slope. Besides, in this case, the UF formula generates shallower river than the CMR formula, mainly due to the differences in the friction and its exponent. However, the situation can change depending on how other factors such as the slope, width, and flow alter. Additionally, the UF river bathymetry is more sensitive to variations in these parameters than the CMR river bathymetry.

The above findings are based on the variation in the river bathymetry when a parameter is changed while others remain constant. Also, we have not considered other factors such as sediment load in this analysis. Hence, these results should not be used to fully reflect the real-world river systems. In the next section, we will observe the changes of these parameters and their simulations along the Waikanae River and how they are correlated with the changes in the corresponding river bathymetries to see if the results match with the findings in this section.

3.2 Findings from evaluating relationships of bathymetry and parameters in the formulas on the study site

To analyse, we divided the distance between Waikanae River Treatment Plant gauge (upstream) and the coast into two parts – from the river upstream to 1000 m downstream, and from 1000 m downstream to the coast. From upstream to 1000 m downstream, Fig. 4a and 4b indicate that the Waikanae river becomes gentler when it also deepens. In this case, despite variability along the river of other parameters like the river width, the relationship between slope and bathymetry still aligns with findings in Section 3.1. Their simulations also follow this trend as seen in Fig. 4c.

In Fig. 4d and 4e, when the Waikanae River becomes deeper from upstream to 1000 m downstream, its flow shows only a slight increase, from 145.3 to 146.2 cumecs, with the highest value remaining constant over a distance of 6000 m downstream. This implies that the bathymetry along this river is not strongly correlated with the bank-full flow. However, in Fig. 4f, the simulated rivers slightly deepens when the simulated flow increases. This pattern is still consistent with observations from Section 3.1, even though other simulated parameters, like width and slope, vary along the river.

In Fig. 4g and 4h, the Waikanae river width resembles a reversed version of its bathymetry, showing an inverse relationship. Although other parameters, especially the slope, also vary along the river, in this case, the relationship of the Waikanae River width and bathymetry still follows the result found in Section 3.1. Their simulations also show this relationship in Fig. 4i.

Figures 4j-m depict the simulated bathymetries using all simulated parameters and their relationships. They all show the same patterns as what we found above when analysing Waikanae River slope, bank-full flow, and width. Specifically, from the upstream to 1000 m downstream, the simulated bathymetries and bank-full flows are not strongly correlated with each
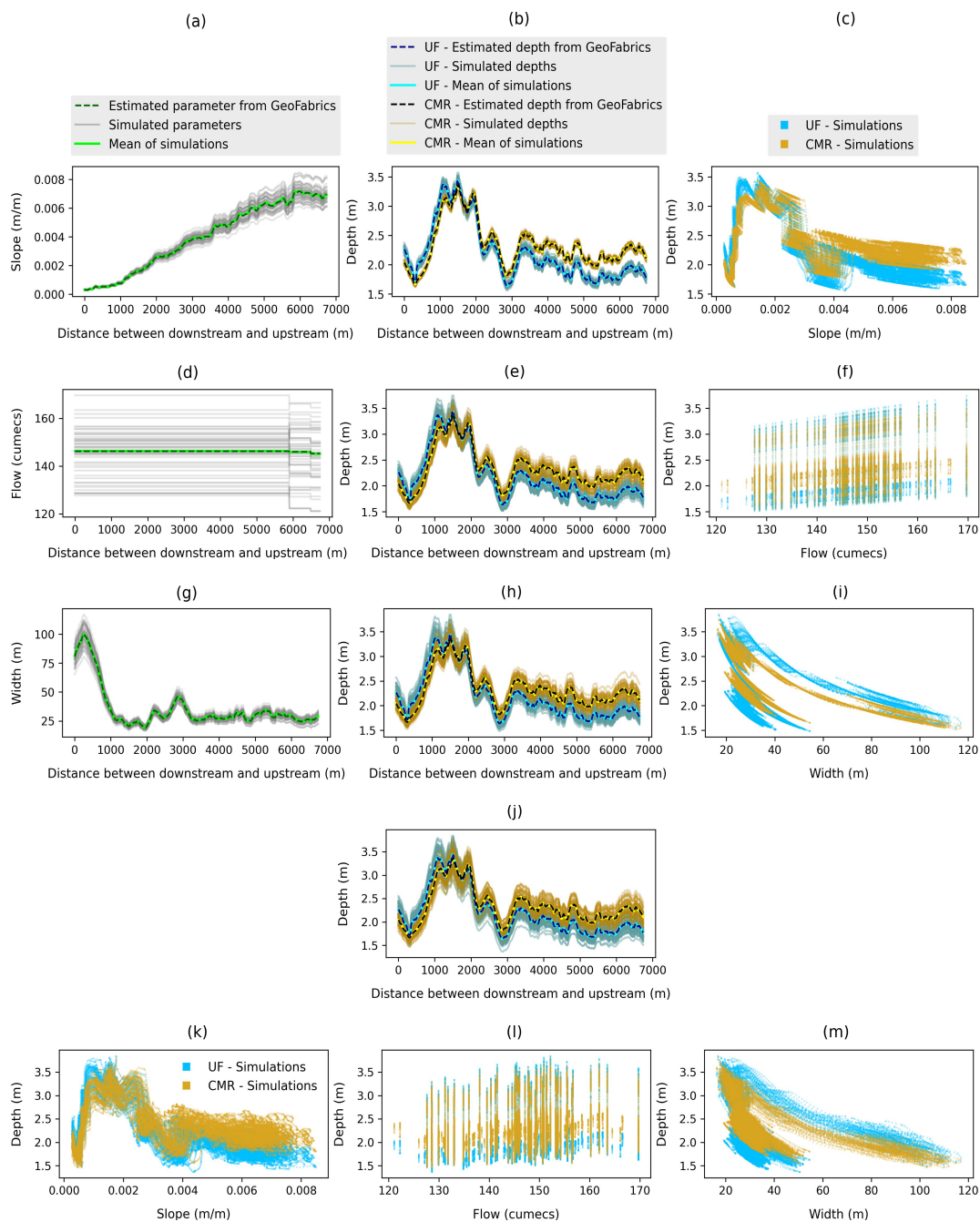
Figure 4. Relationships between simulated Waikanae River slopes, bank-full flows, widths, and bathymetries estimated by the Conceptual Multivariate Regression and Uniform Flow formulas. First row: (a) simulated slopes, (b) corresponding bathymetries, and (c) their relationships. Second row: (d) simulated bank-full flows, (e) corresponding bathymetries, and (f) their relationships. Third row: (g) simulated widths, (h) corresponding bathymetries, and (i) their relationships. Fourth and fifth rows: (j) simulated bathymetries using all simulated parameters, and their relationships with simulated (k) slopes, (l) bank-full flows, and (m) widths.

other. Along the river within the same distance, the simulated river slopes decrease as the simulated bathymetries increase. Finally, the shapes of the simulated river widths are reversed versions of the simulated river bathymetries, showing their inverse relationship.

In Fig. 4b, e, h, and j, from upstream to 1000 m downstream, the river bathymetries estimated by the UF are lower than
250 the CMR formula mainly due to the difference in the friction and its exponent, as explained in Section 3.1. However, from the 1000 m to the coast, both formulas generate shallower rivers in which the bathymetries calculated by the UF formula are greater than the CMR formula. This is where the river slope decreases 80 % from about 0.001 m/m to about 0.0002 m/m. Simultaneously, its width increases up to 400 % from approximately 20 m to around 100 m.

In this region, given the flat terrain, the slope decrease is less correlated with the river bathymetry than the width increase.
255 Mathematically, the slope and width are in the denominator of both formulas, indicating their inverse relationships with the river bathymetries. Furthermore, the slope drop (within 80 %) and its exponents (0.3 and 0.175 for the UF and CMR formulas) are much smaller than the width increase (within 400 %) and its exponents (0.6 and 0.573 for the UF and CMR formulas). Consequently, the river bathymetries are more correlated with the width rise than the slope decrease. Besides, as mentioned in Section 3.1, at this location, when the width starts increasing and the slope keeps decreasing, the river bathymetries of both
260 formulas first converge, then diverge, with the UF bathymetries eventually exceeding the CMR bathymetries.

Figure 5 shows the variations in the simulated bathymetries across the spatial domain when the associated error distributions with the same percentage standard deviation were added into the slope, flow, and width both individually and simultaneously. In both formulas, the ranges of coefficients of variations increases between the slope, flow, and width datasets. It indicates that the variation in the river width is associated with the largest variability in the river bathymetries, followed by the river flow
265 and slope. Moreover, the colours of the UF-formula river bathymetries are darker than those of the CMR-formula ones. This demonstrates the UF-formula bathymetries exhibit larger variability than those from the CMR formula. These all results are consistent with the findings in Section 3.1.

Overall, from the Waikanae River upstream to 1000 m downstream, despite a slight rise in the simulated bathymetries when the simulated flow increase, they are not strongly correlated with each other. Along this distance, the simulated river becomes
270 deeper as their slopes become gentler. The simulated river widths are opposite versions of the simulated bathymetries, demonstrating their inverse relationship. Despite the simultaneous variability along the river of these parameters, their relationships with the bathymetry are still consistent with the findings in Section 3.1. From the 1000 m downstream to the coast, the river becomes shallower when it widens with a mild drop in the slope. Besides, for both formulas, the variation in the river width corresponds to the largest variability in the river bathymetries, followed by the river flow and slope. The
275 UF-formula river bathymetries have more variations than the CMR-formula ones across three parameters. In the next section, we investigated how these variations in the bathymetries affect the flood predictions.

3.3 Comparison of variations in maximum water depths

The variations in covMWDs using the eight datasets are presented in Fig. 6 with their quartile deviations for comparison. We observed that, in both formulas, the slope dataset exhibits the smallest variability in the covMWDs, followed by the flow,
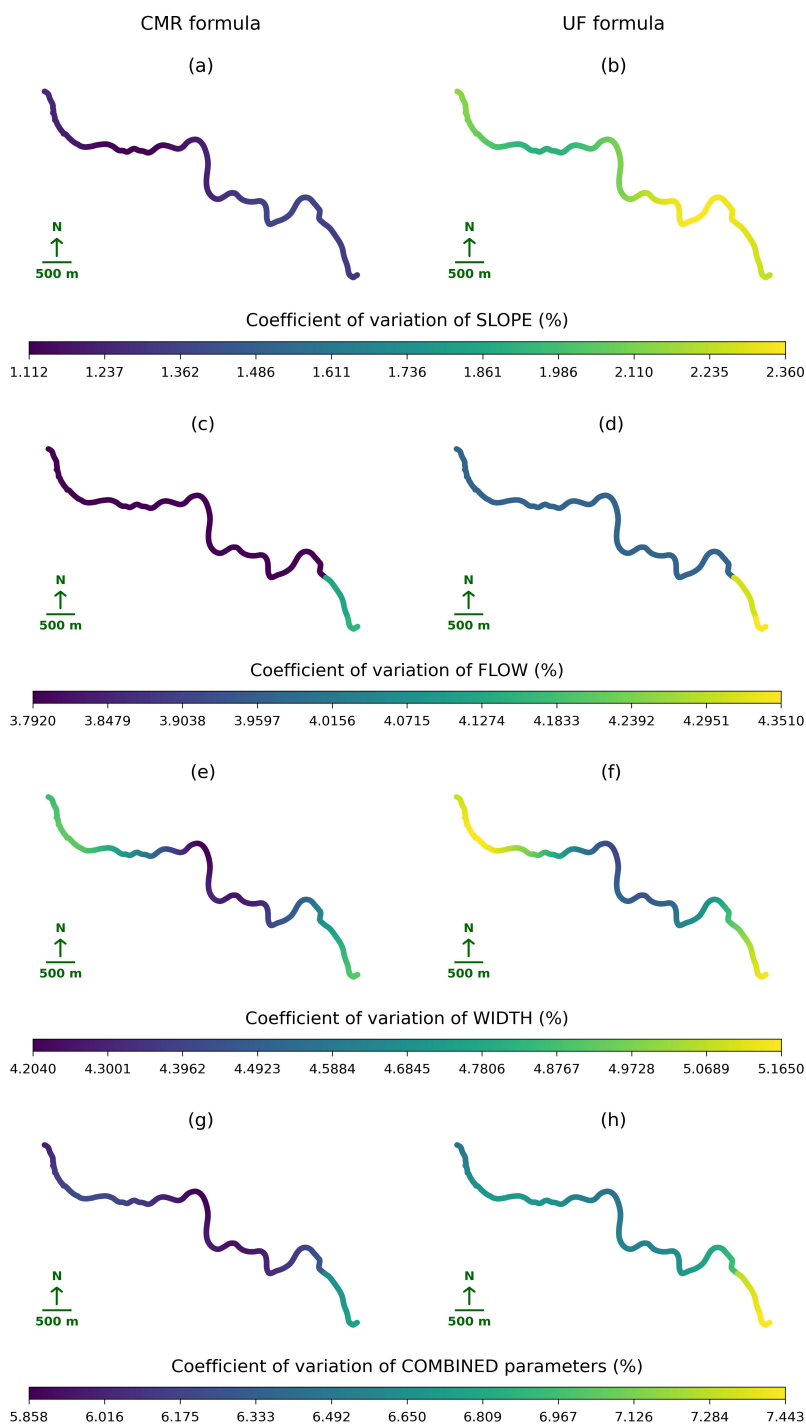
Figure 5. Variations in the simulated Waikanae River bathymetries due to associated error distributions in parameters: the Conceptual Multivariate Regression formula - (a) slope, (c) bank-full flow, (e) width, and (g) combined; the Uniform Flow formula - (b) slope, (d) bank-full flow, (f) width, and (h) combined.
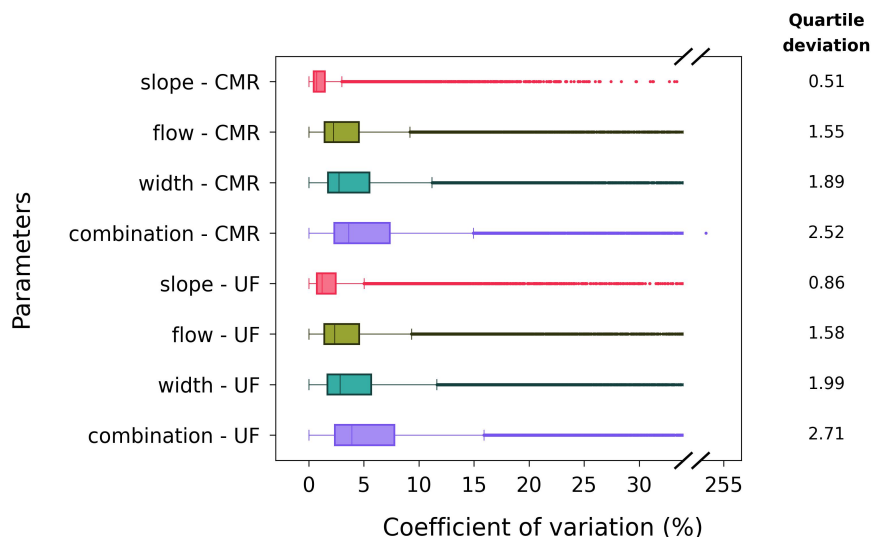
Figure 6. Distributions of coefficients of variations of maximum water depths (covMWDs) for eight datasets (slope-, flow-, width-, and combination-CMR and -UF datasets).

width, and combination datasets. Furthermore, across all parameters, the UF-formula datasets have higher variability in the covMWDs than the CMR-formula datasets.

The order of variation magnitudes between datasets is visible in Fig. 7, especially in the green zoomed in images. Specifically, in both formulas, more locations with covMWDs less than 1.5 % are found in the slope dataset than in the flow, followed by the width, and then the combination datasets. The covMWDs larger than 1.5 % are mainly observed at the edges of the flood extents around midstream and tend to decrease closer to the river. It is also clear in these figures that the datasets using the CMR formula have more locations with covMWDs below 1.5 % than those using the UF formula. For the combination dataset, in the green zoomed-in image, we can see that the colours of covMWDs of the CMR formula are darker than those of the UF formula. These orders of variation magnitudes in flood depths between datasets follow those in the river bathymetries found in Section 3.1 and 3.2.

To explain, between parameter datasets, the small variability in the river bathymetry corresponding with the variation in the river slope does not significantly affect the water spreading into the floodplain, unlike the variations in the river bank-full flow and width. The impacts of all these variations become more apparent in floodplains farther from the river, especially at flood boundaries in midstream, where the water has less direct connection with the river. Between two formulas, because the variations in the UF-formula river bathymetries are higher than the CMR-formula ones as seen in Fig. 5, the variations in the flood depths of the UF-formula datasets are also higher than the CMR-formula datasets.
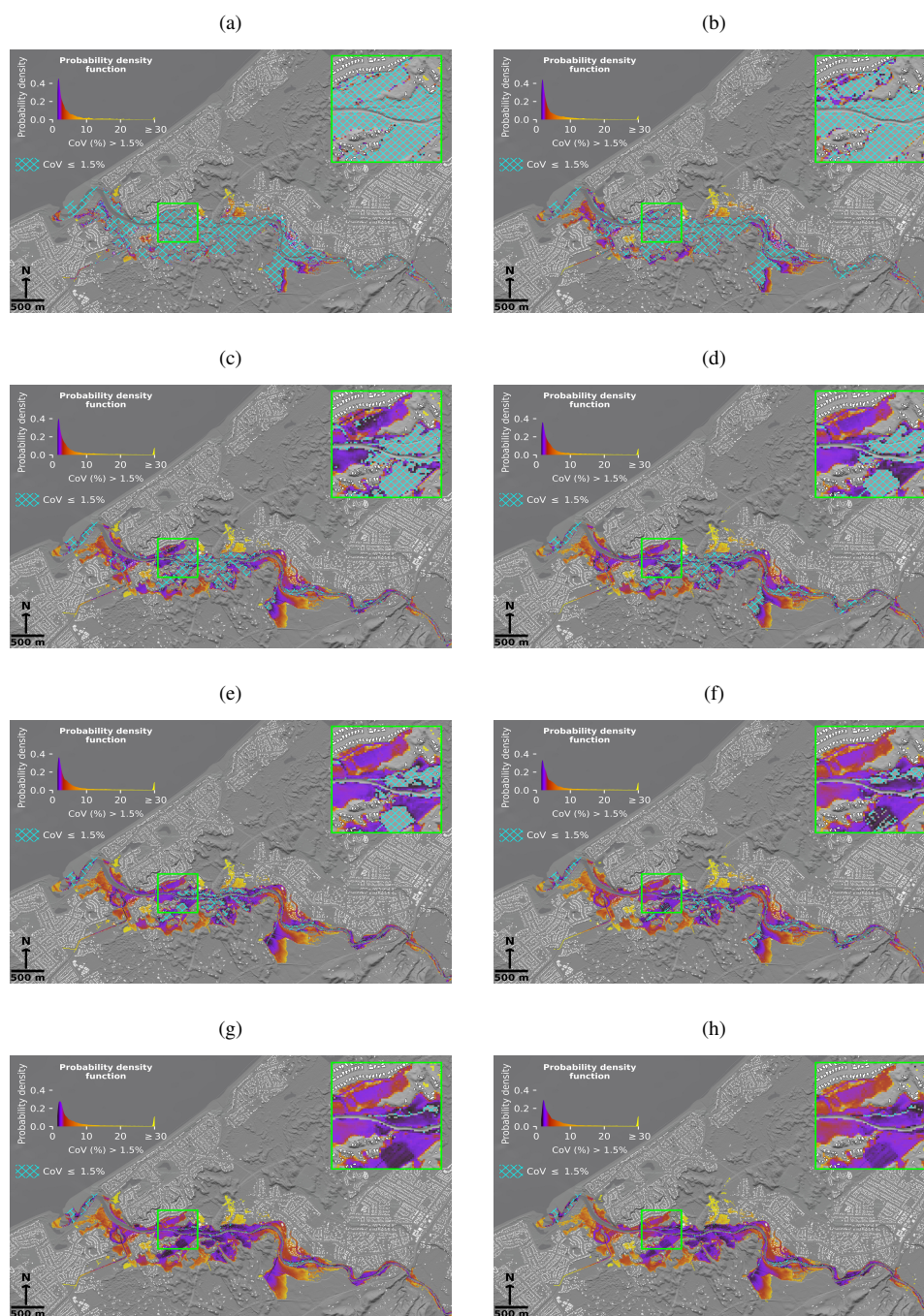
Figure 7. Variations in January-2005 maximum flood depths based on simulated Waikanae River bathymetries estimated by parameters with associated error distributions: the Conceptual Multivariate Regression formula - (a) slope, (c) bank-full flow, (e) width, and (g) combined; the Uniform Flow formula - (b) slope, (d) bank-full flow, (f) width, and (h) combined.
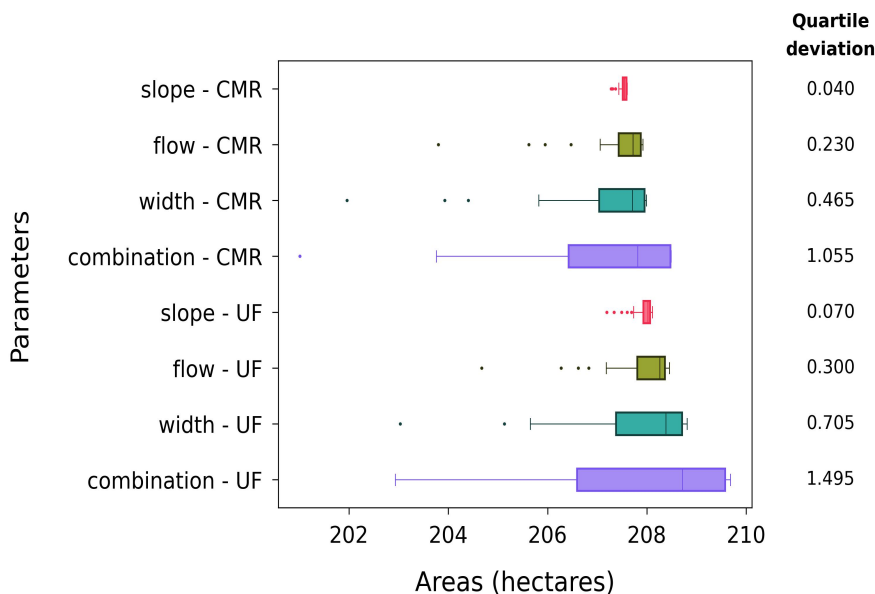
Figure 8. Distributions of flood extent for eight datasets (slope-, flow-, width-, and combination-CMR and -UF datasets).

3.4   Comparison of variations in flood extents

Figure 8 shows a comparison of flood extents between the eight datasets. In both formulas, the slope datasets have the smallest variability in the flood extent followed by the flow, width, and the combination datasets. The order of these variation magnitudes in flood extent between datasets align with those in the river bathymetries, as noted in Section 3.1 and 3.2. The blue zoomed-in
300   images in Fig. 9 can visualize these flood extent differences.

The locations flooded less than 100 % of the time increase between the slope, flow, width, and combination datasets as seen in the blue zoomed-in images of Fig. 9. To explain, the bathymetry determines the water volume the river can hold, which influences how much water can exceed the riverbank and extend in the floodplain. Hence, with the same amount of flood water from the January-2005 event, a small variation in the river bathymetry can result in a small variation in the flood extent
305   and vice versa. This demonstrates the order of variation magnitudes in flood extents between datasets follows that in the river bathymetries.

Between the two formulas, the blue zoomed-in images highlight a location surrounding the river upstream to 1000 m downstream where the UF-formula river bathymetries are lower than the CMR-formula ones, resulting in greater flood extent here in the UF-formula datasets. This leads to that, in the UF-formula datasets, the flood extent variation appears not only in
310   locations already totally flooded in the CMR-formula but also in new regions that are never flooded in the CMR-formula datasets. Consequently, there are more variations in flood extent in the UF-formula datasets compared to the CMR-formula datasets.
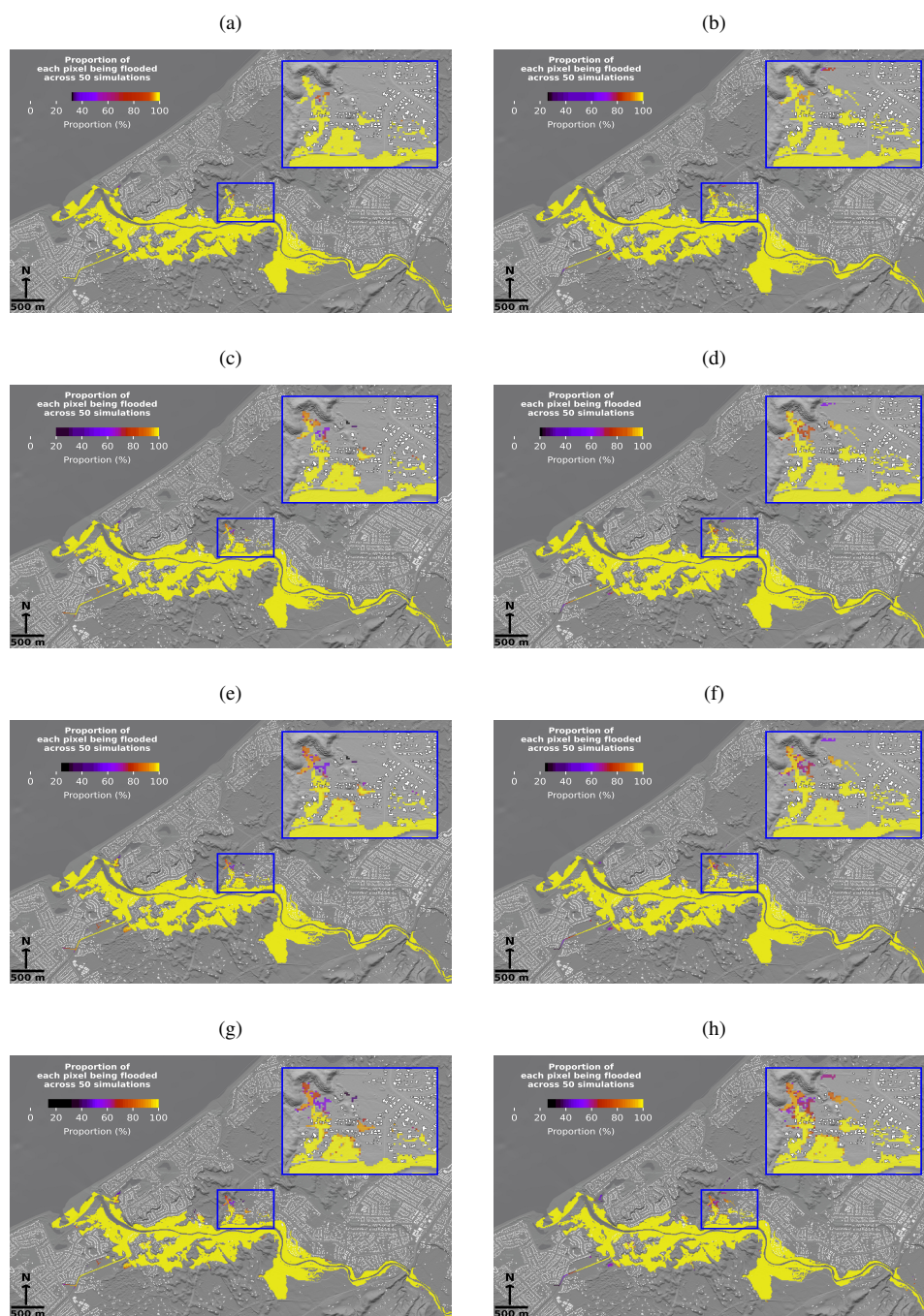
Figure 9. Variations in January-2005 flood extents based on simulated Waikanae River bathymetries estimated by parameters with associated error distributions: the Conceptual Multivariate Regression formula - (a) slope, (c) bank-full flow, (e) width, and (g) combined; the Uniform Flow formula - (b) slope, (d) bank-full flow, (f) width, and (h) combined.
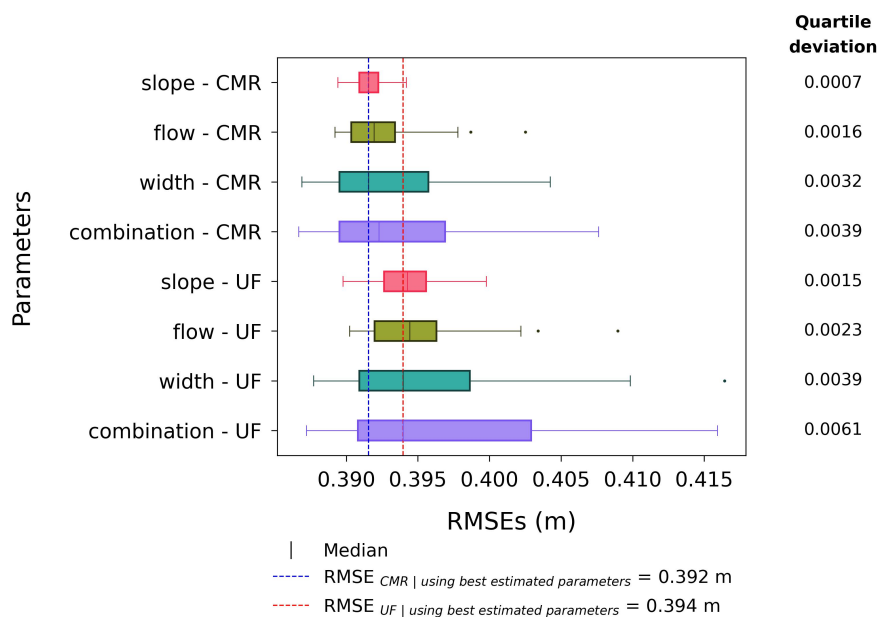
Figure 10. RMSE distributions for predicted flood levels of eight datasets (slope-, flow-, width-, and combination-CMR and -UF datasets) compared to the January-2005 observed flood levels.

3.5 Comparison of variations in RMSEs

Figure 10 shows that, in both formulas, the variation in RMSEs of the slope dataset is the smallest, followed by those of
315 flow, width, and combination datasets. In addition, the variations in RMSEs of the UF-formula datasets are larger than the CMR-formula datasets. These trends correspond to the order of variations in river bathymetries as mentioned in Section 3.1 and 3.2.

The blue and red dashed lines represent the RMSEs for the CMR and UF formulas when using the LiDAR-derived and NIWA-estimated parameters without adding any errors. Each line stands in the middle of boxplots of each formula,
320 demonstrating that these parameters still contain some errors deviating the results from the true predictions. Apart from that, we also noted the UF-formula RMSEs are slightly higher than the CMR-formula ones. To explain, the CMR is developed for coarse-grained rivers like the Waikanae River, leading to lower RMSEs than the UF formula. In contrast, the UF formula was not developed for any specific river types, which may contribute to its slightly higher RMSE. However, these small differences in RMSEs between the two formulas highlight a broad applicability of the UF formula on rivers without
325 categorizing their types.

4 Discussion

Our research went a step further than previous studies to quantify the uncertainty in flood predictions due to the errors in the estimated river bathymetry. We applied the Monte Carlo method and errors selected from Gaussian distributions like Durand et al. (2008); Lee et al. (2018); Kechnit et al. (2024). However, unlike Lee et al. (2018), we selected a larger sample to capture the typical variability in the flood predictions and included the spatial variability into our method. Moreover, we not only considered associated error distributions in parameters collectively like Moramarco et al. (2019); Kechnit et al. (2024), but we also performed a sensitivity analysis to assess each parameter impact.

In our research, we enhance the applicability of our findings by using the UF formula which is not constrained by specific observed data and applicable across a wide range of river types. Our results, based on the slight differences between the CMR and the UF equations, suggest the general applicability of the UF formula without the need of river categorization. However, because we have only compared with the CMR formula, and the real-world river system is complex, this still needs further research.

Our study analysed the errors inherent in three parameters used in the two formulas, but has not explored the errors in the river friction as well as α and β coefficients due to time-intensity and complexity. Furthermore, the Waikanae River bank-full flow is not strongly correlated with the variability of the bathymetry along the river as it nearly stays constant. Hence, future studies should investigate the errors associated with these factors.

Nguyen et al. (2024b) analysed how the grid resolution influences on the flood predictions, which was not considered in our study. The change in grid size can cause a significant change in the river bathymetry and flood results. To capture the river structure with high accuracy, the grid resolution should provide several grid cells across the river. This ensures the river is well resolved for flood modelling. Accordingly, a further study about this is essential for better understanding.

Using the UF and CMR formulas with the best estimated parameters to obtain the river bathymetry can overcome the time-intensive and expensive nature of its acquisition. However, it contains the errors which can affect the flood predictions as our paper analysed above. Currently, without using Monte Carlo framework, a freeboard is often added to the flood level for addressing such uncertainty. It typically considers deviations in flood estimate, construction tolerances, and natural factors not accounted for in the calculations (Ministry for the Environment, 2024). However, this technique does not account for variations in flood extents, as demonstrated in Section 3.4 in this research, which can be influenced by the estimated river bathymetry. This suggests a future investigation to improve the effectiveness of this technique.

On the other hand, applying the Monte Carlo framework to quantify this uncertainty is more effective. However, its process is complicated, resource-intensive, and time-consuming. Hence, a simpler and faster approach is essential. Machine learning approach, well-known for its fast and simpler process to obtain the comparable results, is a good candidate which needs further investigation.

5 Conclusions

Our research focused on quantifying the uncertainty in flood predictions due to the errors in parameters used to estimate the river
bathymetries. We applied LISFLOOD-FP flood model within a Monte Carlo method to generate multiple flood simulations for
the January-2005 Waikanae River flood event for analysis. We performed a sensitivity analysis on three estimated parameters
(river slope, flow, and width) and two formulas (the UF and CMR formulas) to assess their error impacts on the flood predictions
individually and collectively through the estimated river bathymetries.

Among the three parameters, when the simulated errors with the same percentage standard deviation were added to each of
them, the variation in the width corresponds to the highest variability in the river bathymetries, followed by the flow and slope
datasets. Between two formulas, river bathymetries estimated by the UF formula exhibit greater variations than those estimated
by the CMR formula. These variations in the river bathymetries are reflected in the flood predictions: the slope dataset has
the lowest variability in flood depths and flooded areas, resulting in narrower ranges of RMSEs, while the width dataset has
the highest variability. Additionally, the UF-formula datasets show greater variations in flood depths and extents, with more
variations in RMSEs compared to the CMR formula.

The slight differences in RMSEs between the two formulas suggest a broad applicability of the UF formula across many
river types without categorizing them, but another study is still necessary for confirming this potential. Apart from that, future
research should also consider the impacts of grid resolution on the estimated river bathymetry, which then influences on the
flood predictions. Furthermore, our research did not account for the associated error distributions in the river friction, α and β
coefficients, and fluctuated flow rate along the river. Hence, these factors need to be further investigated for better understanding
their impacts on the flood predictions. Currently, to cover such uncertainty, a freeboard is used but it fails to cover the variation
in the flood extent, and thus a further study is needed to improve its effectiveness. Lastly, there is a need for simpler and faster
method than Monte Carlo framework such as machine learning approaches.

Code and data availability. The project employed GeoFabrics package and the flood model LISFLOOD-FP developed by Pearson et al.
(2023) and Bates et al. (2010) respectively. All necessary data for simulation generation and results have been saved at Nguyen et al. (2024a)

Author contributions. Based on the Contributor Role Taxonomy: Conceptualization - MN, MW, and EL; Funding acquisition - MW and EL,
Formal analysis - MN, Data curation - MN, Methodology - MN, MW, EL, JB, and RP, Software - MN, RP, Supervision - MW, EL, and JB,
Writing original draft - MN, Writing - review & editing - MW, EL, JB, and RP

Competing interests. The authors declare that they have no conflict of interest.

Acknowledgements. The project was sponsored by the Ministry for Business, Innovation and Employment as a PhD scholarship awarded to
385 Martin Nguyen through the New Zealand flood hazard assessment programme, "Reducing flood inundation hazard and risk across Aotearoa
– New Zealand". It is led by NIWA in collaboration with Geospatial Research Institute, School of Earth and Environment, University of
Canterbury in Christchurch, New Zealand.

References

Alessandrini, V., Bernardi, G., and Todini, E.: An operational approach to real-time dynamic measurement of discharge, Hydrology Research, 44, 953–964, https://doi.org/10.2166/nh.2013.138, 2013.

Andreadis, K. M., Schumann, G. J.-P., and Pavelsky, T.: A simple global river bankfull width and depth database, Water Resources Research, 49, 7164–7168, https://doi.org/10.1002/wrcr.20440, 2013.

Andreadis, K. M., Brinkerhoff, C. B., and Gleason, C. J.: Constraining the Assimilation of SWOT Observations With Hydraulic Geometry Relations, Water Resources Research, 56, e2019WR026 611, https://doi.org/10.1029/2019WR026611, 2020.

Araújo, A. and Hedley, N.: Bathymetric data visualization – A review of current methods, practices and emerging interface opportunities, The International Hydrographic Review, 29, 150–163, https://doi.org/10.58440/ihr-29-2-a29, 2023.

Awadallah, M. O. M., Juárez, A., and Alfredsen, K.: Comparison between Topographic and Bathymetric LiDAR Terrain Models in Flood Inundation Estimations, Remote Sensing, 14, 227, https://doi.org/10.3390/rs14010227, 2022.

Bailly, J.-S., Le Coarer, Y., Languille, P., Stigermark, C.-J., and Allouis, T.: Geostatistical estimations of bathymetric LiDAR errors on rivers, Earth Surface Processes and Landforms, 35, 1199–1210, https://doi.org/10.1002/esp.1991, 2010.

Bates, P. D., Horritt, M. S., and Fewtrell, T. J.: A simple inertial formulation of the shallow water equations for efficient two-dimensional flood inundation modelling, Journal of Hydrology, 387, 33–45, https://doi.org/10.1016/j.jhydrol.2010.03.027, 2010.

Bhuyian, M. N. M., Kalyanapu, A. J., and Nardi, F.: Approach to Digital Elevation Model Correction by Improving Channel Conveyance, Journal of Hydrologic Engineering, 20, 04014 062, https://doi.org/10.1061/(ASCE)HE.1943-5584.0001020, 2015.

Brown, R. A., Pasternack, G. B., and Wallender, W. W.: Synthetic river valleys: Creating prescribed topography for form–process inquiry and river rehabilitation design, Geomorphology, 214, 40–55, https://doi.org/10.1016/j.geomorph.2014.02.025, 2014.

Brêda, J. P. L. F., Paiva, R. C. D., Bravo, J. M., Passaia, O. A., and Moreira, D. M.: Assimilation of Satellite Altimetry Data for Effective River Bathymetry, Water Resources Research, 55, 7441–7463, https://doi.org/10.1029/2018WR024010, 2019.

Bures, L., Sychova, P., Maca, P., Roub, R., and Marval, S.: River Bathymetry Model Based on Floodplain Topography, Water, 11, 1287, https://doi.org/10.3390/w11061287, 2019.

Coe, M., Costa, M., and Howard, E.: Simulating the surface waters of the Amazon River basin: Impacts of new river geomorphic and flow parameterizations, Hydrological Processes, 22, 2542–2553, https://doi.org/10.1002/hyp.6850, 2008-07.

Cook, A. and Merwade, V.: Effect of topographic data, geometric configuration and modeling approach on flood inundation mapping, Journal of Hydrology, 377, 131–142, https://doi.org/10.1016/j.jhydrol.2009.08.015, 2009.

Costa, B. M., Battista, T. A., and Pittman, S. J.: Comparative evaluation of airborne LiDAR and ship-based multibeam SoNAR bathymetry and intensity for mapping coral reef ecosystems, Remote Sensing of Environment, 113, 1082–1100, https://doi.org/10.1016/j.rse.2009.01.015, 2009.

Dey, S., Saksena, S., and Merwade, V.: Assessing the effect of different bathymetric models on hydraulic simulation of rivers in data sparse regions, Journal of Hydrology, 575, 838–851, https://doi.org/10.1016/j.jhydrol.2019.05.085, 2019.

Durand, M., Andreadis, K. M., Alsdorf, D. E., Lettenmaier, D. P., Moller, D., and Wilson, M.: Estimation of bathymetric depth and slope from data assimilation of swath altimetry into a hydrodynamic model, Geophysical Research Letters, 35, https://doi.org/10.1029/2008GL034150, 2008.

Flener, C., Lotsari, E., Alho, P., and Käyhkö, J.: Comparison of empirical and theoretical remote sensing based bathymetry models in river environments, River Research and Applications, 28, 118–133, https://doi.org/10.1002/rra.1441, 2012.

425 Garambois, P.-A. and Monnier, J.: Inference of effective river properties from remotely sensed observations of water surface, Advances in Water Resources, 79, 103–120, https://doi.org/10.1016/j.advwatres.2015.02.007, 2015.

Ghorbanidehno, H., Lee, J., Farthing, M., Hesser, T., Darve, E. F., and Kitanidis, P. K.: Deep learning technique for fast inference of large-scale riverine bathymetry, Advances in Water Resources, 147, 103 715, https://doi.org/10.1016/j.advwatres.2020.103715, 2021.

Gichamo, T. Z., Popescu, I., Jonoski, A., and Solomatine, D.: River cross-section extraction from the ASTER global DEM for flood modeling,
430 Environmental Modelling & Software, 31, 37–46, https://doi.org/10.1016/j.envsoft.2011.12.003, 2012.

Gleason, C. J. and Smith, L. C.: Toward global mapping of river discharge using satellite images and at-many-stations hydraulic geometry, Proceedings of the National Academy of Sciences, 111, 4788–4791, https://doi.org/10.1073/pnas.1317606111, 2014.

Greater Wellington Regional Council: Environmental Data Dashboard - Release 2.5, https://graphs.gw.govt.nz/envmon?view=graph&collection=All+Data+Types&site=Waikanae+River+at+Water+Treatment+Plant&measurement=Flow&flow=Measured+Flow, 2005.

435 Grimaldi, S., Li, Y., Walker, J. P., and Pauwels, V. R. N.: Effective Representation of River Geometry in Hydraulic Flood Forecast Models, Water Resources Research, 54, 1031–1057, https://doi.org/10.1002/2017WR021765, 2018.

Gräler, B., Pebesma, E., and Heuvelink, G.: Spatio-Temporal Interpolation using gstat, The R Journal, 8, 204–218, https://journal.r-project.org/archive/2016/RJ-2016-014/index.html, 2016.

Gyopari, M., Mzila, D., and Hughes, B.: Kaipiti Coast groundwater resource investigation:
440 Catchment hydrogeology and modelling report, https://www.gw.govt.nz/assets/Documents/2014/10/Kapiti-Coast-groundwater-resource-investigation-Catchment-hydrogeology-and-modelling-report.pdf, 2014.

Henderson and Collins: New Zealand River Flood Statistics App, https://data-niwa.opendata.arcgis.com/apps/NIWA::new-zealand-river-flood-statistics-app/explore, 2018.

Huang, H., Liao, W., Lei, X., Wang, C., Cai, Z., and Wang, H.: An urban DEM reconstruction method based on multisource data fusion for
445 urban pluvial flooding simulation, Journal of Hydrology, 617, 128 825, https://doi.org/10.1016/j.jhydrol.2022.128825, 2023.

Ibrahim, F. and Fritsch, D.: Flood Spatial Analysis Using LiDAR DEM Study Area (Azozab locality-Khartoum state-Sudan), Int. J. Comput. Sci. Trends Technol, 10, 122–133, 2022.

Kechnit, D., Tshimanga, R. M., Ammari, A., Trigg, M. A., Carr, A. B., Bahmanpouri, F., Barbetta, S., and Moramarco, T.: Bathymetry and discharge estimation in large and data-scarce rivers using an entropy-based approach, Hydrological Sciences Journal, 0, 1–15,
450 https://doi.org/10.1080/02626667.2024.2402933, 2024.

Kinzel, P. J., Legleiter, C. J., and Nelson, J. M.: Mapping River Bathymetry With a Small Footprint Green LiDAR: Applications and Challenges, JAWRA Journal of the American Water Resources Association, 49, 183–204, https://doi.org/10.1111/jawr.12008, 2013.

Lee, J., Ghorbanidehno, H., Farthing, M. W., Hesser, T. J., Darve, E. F., and Kitanidis, P. K.: Riverine Bathymetry Imaging With Indirect Observations, Water Resources Research, 54, 3704–3727, https://doi.org/10.1029/2017WR021649, 2018.

455 Leopold, L. B. and Jr, T. M.: The hydraulic geometry of stream channels and some physiographic implications, Professional Paper, https://doi.org/10.3133/pp252, 1953.

López, R., Barragán, J., and Colomer, M. A.: Flow resistance equations without explicit estimation of the resistance coefficient for coarse-grained rivers, Journal of Hydrology, 338, 113–121, https://doi.org/10.1016/j.jhydrol.2007.02.027, 2007.

Miguez-Macho, G. and Fan, Y.: The role of groundwater in the Amazon water cycle: 1. Influence on seasonal streamflow, flooding and
460 wetlands, Journal of Geophysical Research: Atmospheres, 117, https://doi.org/10.1029/2012JD017539, 2012.

Ministry for the Environment: Coastal hazards and climate change guidance, https://environment.govt.nz/assets/publications/Coastal-hazards-and-climate-change-guidance-2024-ME-1805.pdf, 2024.

Moramarco, T. and Singh, V. P.: Formulation of the Entropy Parameter Based on Hydraulic and Geometric Characteristics of River Cross Sections, Journal of Hydrologic Engineering, 15, 852–858, https://doi.org/10.1061/(ASCE)HE.1943-5584.0000255, 2010.

465 Moramarco, T., Barbetta, S., Bjerklie, D. M., Fulton, J. W., and Tarpanelli, A.: River Bathymetry Estimate and Discharge Assessment from Remote Sensing, Water Resources Research, 55, 6692–6711, https://doi.org/10.1029/2018WR024220, 2019.

Neal, J., Schumann, G., and Bates, P.: A subgrid channel model for simulating river hydraulics and floodplain inundation over large and data sparse areas, Water Resources Research, 48, https://doi.org/10.1029/2012WR012514, 2012.

Neal, J., Dunne, T., Sampson, C., Smith, A., and Bates, P.: Optimisation of the two-dimensional hydraulic model LISFOOD-FP for CPU

470 architecture, Environmental Modelling & Software, 107, 148–157, https://doi.org/10.1016/j.envsoft.2018.05.011, 2018.

Neal, J., Hawker, L., Savage, J., Durand, M., Bates, P., and Sampson, C.: Estimating River Channel Bathymetry in Large Scale Flood Inundation Models, Water Resources Research, 57, e2020WR028 301, https://doi.org/10.1029/2020WR028301, 2021.

Nguyen, M., Wilson, M. D., Lane, E. M., Brasington, J., and Pearson, R.: Quantifying uncertainty in flood predictions due to river bathymetry estimation - Results and Github, https://doi.org/10.26021/canterburynz.27644997.v1, 2024a.

475 Nguyen, M., Wilson, M. D., Lane, E. M., Brasington, J., and Pearson, R. A.: Quantifying uncertainty in flood predictions in LISFLOOD-FP due to arbitrary conventions in grid alignment in LiDAR-derived digital elevation models [Manuscript submitted for publication], Geospatial Research Institute, School of Earth and Environment, University of Canterbury, New Zealand, 2024b.

NIWA Tide Forecaster: NIWA's Tide Forecaster provides tidal data for any point in New Zealand, https://tides.niwa.co.nz/?latitude=-40. 866&longitude=174.987&datum=MSL&interval=10&startDate=2005-01-01&numberOfDays=31, 2005.

480 OpenTopography: Wellington, New Zealand 2013-2014, https://doi.org/10.5069/g9cv4fpt, 2013.

Panigrahi, N.: An Introduction to Bathymetry, in: Computing in Geographic Information Systems, CRC Press, ISBN 9780429069635, 2014.

Pearson, R. A., Smart, G., Wilkins, M., Lane, E., Harang, A., Bosserelle, C., Cattoën, C., and Measures, R.: GeoFabrics 1.0.0: An open-source Python package for automatic hydrological conditioning of digital elevation models for flood modelling, Environmental Modelling & Software, 170, 105 842, https://doi.org/10.1016/j.envsoft.2023.105842, 2023.

485 Pebesma, E. J.: Multivariable geostatistics in S: the gstat package, Computers and Geosciences, 30, 683–691, 2004.

Price, R. K.: An optimized routing model for flood forecasting, Water Resources Research, 45, https://doi.org/10.1029/2008WR007103, 2009.

Rupp, D. E. and Smart, G. M.: Comment on "Flow resistance equations without explicit estimation of the resistance coefficient for coarse-grained rivers" by Raúl López, Javier Barragán, and M. Àngels Colomer, Journal of Hydrology, 346, 174–178,

490 https://doi.org/10.1016/j.jhydrol.2007.08.024, 2007.

Saleh, F., Ducharne, A., Flipo, N., Oudin, L., and Ledoux, E.: Impact of river bed morphology on discharge and water levels simulated by a 1D Saint–Venant hydraulic model at regional scale, Journal of Hydrology, 476, 169–177, https://doi.org/10.1016/j.jhydrol.2012.10.027, 2013.

Sampson, C. C., Smith, A. M., Bates, P. D., Neal, J. C., Alfieri, L., and Freer, J. E.: A high-resolution global flood hazard model, Water

495 Resources Research, 51, 7358–7381, https://doi.org/10.1002/2015WR016954, 2015.

Shannon, C. E.: A mathematical theory of communication, The Bell System Technical Journal, 27, 379–423, https://doi.org/10.1002/j.1538-7305.1948.tb01338.x, 1948.

Smart, G. M.: Improving flood hazard prediction models, International Journal of River Basin Management, 16, 449–456, https://doi.org/10.1080/15715124.2017.1411923, 2018.

500   Trigg, M. A., Wilson, M. D., Bates, P. D., Horritt, M. S., Alsdorf, D. E., Forsberg, B. R., and Vega, M. C.: Amazon flood wave hydraulics, Journal of Hydrology, 374, 92–105, https://doi.org/10.1016/j.jhydrol.2009.06.004, 2009.

Wallace, P.: Waikanae River Hydraulic Model Update 2010, River Edge Consulting Limited, 2010.

Xing, Y., Chen, H., Liang, Q., and Ma, X.: Improving the performance of city-scale hydrodynamic flood modelling through a GIS-based DEM correction method, Natural Hazards, 112, 1–23, https://doi.org/10.1007/s11069-022-05267-1, 2022.

505   Yamazaki, D., de Almeida, G. A. M., and Bates, P. D.: Improving computational efficiency in global river models by implementing the local inertial flow equation and a vector-based river network map, Water Resources Research, 49, 7221–7235, https://doi.org/10.1002/wrcr.20552, 2013.